Research Article | Vol. 31, No. 13 / 19 Jun 2023 / Optics Express 20812
Optics EXPRESS

Vector valley Hall edge solitons in distorted type-II Dirac photonic lattices

YIQING TIAN,[1] YUDIAN WANG,[2] MILIVOJ R. BELIĆ,[3] YIQI ZHANG,[1,5] YONGDONG LI,[1] AND FANGWEI YE[4,6]

[1]*Key Laboratory for Physical Electronics and Devices of the Ministry of Education & Shaanxi Key Lab of Information Photonic Technique, School of Electronic and Information Engineering, Xi'an Jiaotong University, Xi'an 710049, China*
[2]*School of Materials Science and Engineering, Shanghai Jiao Tong University, Shanghai 200240, China*
[3]*Division of Arts and Sciences, Texas A&M University at Qatar, P.O. Box 23874 Doha, Qatar*
[4]*School of Physics and Astronomy, Shanghai Jiao Tong University, Shanghai 200240, China*
[5]*zhangyiqi@xjtu.edu.cn*
[6]*fangweiye@sjtu.edu.cn*

Abstract: Topological edge states have recently garnered a lot of attention across various fields of physics. The topological edge soliton is a hybrid edge state that is both topologically protected and immune to defects or disorders, and a localized bound state that is diffraction-free, owing to the self-balance of diffraction by nonlinearity. Topological edge solitons hold great potential for on-chip optical functional device fabrication. In this report, we present the discovery of vector valley Hall edge (VHE) solitons in type-II Dirac photonic lattices, formed by breaking lattice inversion symmetry with distortion operations. The distorted lattice features a two-layer domain wall that supports both in-phase and out-of-phase VHE states, appearing in two different band gaps. Superposing soliton envelopes onto VHE states generates bright-bright and bright-dipole vector VHE solitons. The propagation dynamics of such vector solitons reveal a periodic change in their profiles, accompanied by the energy periodically transferring between the layers of the domain wall. The reported vector VHE solitons are found to be metastable.

1. Introduction

The topological insulator is a new phase of matter, possessing topologically-protected edge states that are immune to disorders or defects [1,2]. The concept of topological insulator extends beyond condensed matter physics and has led to tremendous interesting phenomena in other areas of physics as well [3–20]. Since their ability to introduce nonlinearity and non-Hermiticity, optical systems have proven to be a useful tool in investigating the topological phase transition and constructing photonic topological insulators [21–23]. The interplay between nonlinearity and topological insulation has led to various phenomena, such as the bistability effects in edge states of pumped dissipative systems [24–26], the breakdown of topological transport [27–29], the birth of nonlinear localized states thanks to the modulation instability of the edge states [30,31], and the stabilization of the operation of topological lasers due to nonlinear gain saturation [32–39] as well as the nonlinearity-induced topological transitions [40]. Additionally, a rich variety of solitonic effects have been observed [41–43], including the formation of self-sustained localized states in the bulk of topological insulators [44,45], nonlinear vortices [46], topological edge solitons [47–62], and topological Bragg solitons [63]. Nonlinearity-induced higher-order topological phases have been observed too [64–66].

Topological edge solitons inherit topological protection property from the topological edge states and maintain their shape during propagation, making them both free from radiation and diffraction. Topological edge states have been reported in both longitudinally modulated waveguide arrays with the effective time-reversal symmetry broken [47–49,52–55], and straight

#491719 https://doi.org/10.1364/OE.491719
Journal © 2023 Received 28 Mar 2023; revised 11 May 2023; accepted 25 May 2023; published 6 Jun 2023

Optics EXPRESS

waveguide arrays with the effective time-reversal symmetry preserved but with the inversion symmetry broken [56–62].

Previous research on topological edge solitons has mainly focused on single-layer edges or interfaces. These edges or interfaces, which can take various forms such as armchair, zigzag, bearded, etc., have usually been studied in their simplest realization, without coupling two armchairs or other types of edges to create more complex interfaces. However, these simple interfaces do not allow for the study of higher-order localized modes, which are essential for exploring the rich physics of interface state coupling.

In this study, our objective is to investigate the formation of coupled localized interfacial states in a type-II Dirac photonic lattice by considering a two-layer edge. The intra-coupling between the two layers of the edge leads to the formation of in-phase and out-of-phase valley Hall edge (VHE) interfacial states, which are situated in different photonic gaps of the Dirac photonic lattices. Additionally, we examine the optically nonlinear effect on the two VHE states, which nonlinearly couples the two fundamental VHE states and localizes them along the interfaces. This localization results in the formation of a vector topological soliton that oscillates coherently between the two layers of the edge, a property that cannot occur in simple interfaces.

2. Results

2.1. Band structure

The propagation of VHE states along the longitudinal z axis of a nonlinear waveguide array can be described by the dimensionless nonlinear Schrödinger-like paraxial wave equation with an external potential and focusing cubic nonlinearity:

$$i\frac{\partial\psi}{\partial z} = -\frac{1}{2}\left(\frac{\partial^2}{\partial x^2} + \frac{\partial^2}{\partial y^2}\right)\psi - \mathcal{R}(x,y)\psi - |\psi|^2\psi, \tag{1}$$

where ψ is the slowly-varying field amplitude, x and y are the normalized transverse coordinates, and z is the normalized propagation distance, given in Rayleigh ranges. The potential function $\mathcal{R}$ describes the waveguide array that is arranged within a type-II Dirac photonic landscape without any modulation along the longitudinal coordinate. The profiles of individual waveguides in the array are represented by Gaussian functions of width σ:

$$\mathcal{R}(x,y) = p\sum_{m,n}\exp\left[-\frac{(x-x_{m,n})^2 + (y-y_{m,n})^2}{\sigma^2}\right], \tag{2}$$

where $p \sim \delta n$ stands for the depth of each site, which is the same for all sites, and $(x_{m,n}, y_{m,n})$ are the coordinates of the nodes in the lattice grid. We consider a configuration that is periodic along the y axis and is limited along the x axis, with outer boundaries located far away from the domain wall, so that $\mathcal{R}(x,y) = \mathcal{R}(x,y+a)$, with a being the array constant, i.e., the distance between two nearest sites. Representative parameter values for these quantities are $a = 1.6$ and $\sigma = 0.5$. Here, the average refractive index modulation depth is set to be $p_{\text{in}} = 10$ which ensures that each channel is single-mode.

Assuming that waveguide arrays are prepared using the femtosecond laser writing technique in fused silica [65,67–70], the normalized parameters described above can be easily switched to experimental values. Provided that the laser radiation at the wavelength of 800 nm is used and the characteristic transverse scale is set to 10 μm, which corresponds to the dimensionless coordinate units $x, y = 1$, the array constant is 16 μm, the waveguide width is 5 μm, and $p = 10$ corresponds to the refractive index modulation depth of $\delta n \sim 1 \times 10^{-3}$.

As usual, the energy band structure is obtained by ignoring the nonlinearity and assuming an ansatz $\psi(x,y,z) = u(x,y)\exp[i(k_y y + bz)]$. After inserting into Eq. (1), one obtains an eigenvalue

Optics EXPRESS

problem:

$$\beta u = \frac{1}{2}\left(\frac{\partial^2}{\partial x^2} + \frac{\partial^2}{\partial y^2} + 2ik_y\frac{\partial}{\partial y} - k_y^2\right)u + \mathcal{R}u, \tag{3}$$

where $u(x, y) = u(x, y + a)$ is the periodic Bloch wave function, $k_y \in [-\mathrm{K}/2, \mathrm{K}/2)$ is the Bloch momentum in the first Brillouin zone, with $\mathrm{K} = 2\pi/a$, and b is the propagation constant of the linear mode that is a function of k_y. The band structure corresponding to the given lattice is then calculated utilizing the plane-wave expansion method.

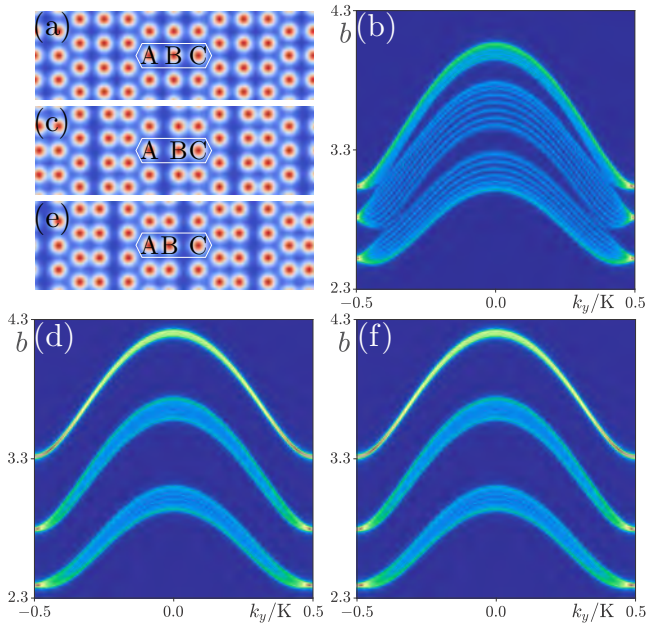

Fig. 1. (a) Type-II Dirac photonic lattice with three sites in each unit cell, marked by letters A, B and C, and with the distance between two nearest neighbor sites 1.6. (b) Band structure projected onto the (k_y, b) plane that corresponds to (a). Two type-II Dirac points connect two neighboring bulk bands. The color scale represents the density of states. (c) Distorted type-II Dirac photonic lattice, with site B being closer to site C. The distance between A and B is 1.9, while that between B and C is 1.3. (d) Band structure projected onto the (k_y, b) plane that corresponds to (c). The type-II Dirac cones disappear and band gaps open. (e) Distorted type-II Dirac photonic lattice, with site B being closer to site A. The distance between A and B is 1.3, while that between B and C is 1.9. (f) Band structure projected onto the (k_y, b) plane that corresponds to (e).

In Fig. 1(a), we display the type-II Dirac photonic lattice that possesses three sites in the unit cell (as indicated by the white hexagon). For ease of discussion, we label the three sites as A, B and C. The corresponding band structure is shown in Fig. 1(b), projected on the plane (k_y, b). In the band structure, we illustrate the density of states by the color scale. One finds clearly that there are two type-II Dirac points, which connect two bulk bands [56,61,71]. To break the inversion symmetry of the lattice, we adjust the location of site B, to make it closer to site A or site C, as shown in Figs. 1(c) and 1(e). The corresponding band structures are shown in Figs. 1(d) and 1(f), respectively. The type-II Dirac cones disappear, because the inversion symmetry is broken—and consequently wide band gaps appear. It is also clear that the band structures in Figs. 1(d) and 1(f) look the same, which is crucial for the establishment of a domain wall that supports VHE states, based on the two inversion-symmetry-broken lattices [72].

Optics EXPRESS

2.2. Theoretical analysis

The theoretical analysis proceeds as follows. According to the bulk-edge correspondence principle, the appearance of valley Hall edge states on the domain wall demands that the valley Chern numbers should be $\pm 1/2$ or $\mp 1/2$ across the domain wall [73,74]. To demonstrate this property in type-II Dirac photonic lattice, we adopt the tight-binding method, with only the nearest-neighbor hopping considered. The form of the lattice is shown in Fig. 2(a), with three sites in the unit cell marked again by A, B and C. Since we adjust the hopping strength between sites A and B and that between sites B and C, we denote the hopping strength between sites A and B as t_1 (red bonds), while that between sites B and C as t_2 (green bonds). The hopping strength between other sites is t (blue bonds). We choose $\mathbf{v}_1 = [2 + \sqrt{3}/2, 0]a$ and $\mathbf{v}_2 = [0, 1]a$ as the basis vectors of the Bravais lattice. Then, the Hamiltonian can be written as:

$$\mathcal{H} = 2t\cos(\mathbf{k}\cdot\mathbf{v}_2)\mathbf{I} + \mathbf{M} + \mathbf{M}^{\mathrm{H}}, \tag{4}$$

where $\mathbf{I}$ is a 3×3 unit matrix, $\mathbf{k} = [k_x, k_y]$, the superscript H indicates the complex conjugate transpose operation, and matrix $\mathbf{M}$ is of the form:

$$\mathbf{M} = \begin{bmatrix} 0 & t_1 & m \\ 0 & 0 & t_2 \\ 0 & 0 & 0 \end{bmatrix}, \tag{5}$$

with $m = 2t\exp(i\mathbf{k}\cdot\mathbf{v}_1)\cos(\mathbf{k}\cdot\mathbf{v}_2/2)$.

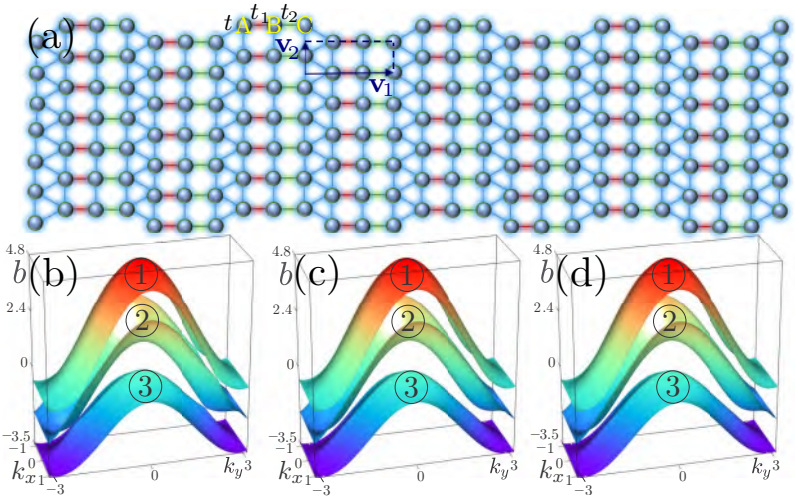

Fig. 2. (a) Form of the type-II Dirac photonic lattice with t, t_1 and t_2 being hopping strengths that correspond to blue bonds, red bonds and green bonds, respectively. The basis vectors of the Bravais lattice are $\mathbf{v}_1 = [2 + \sqrt{3}/2, 0]a$ and $\mathbf{v}_2 = [0, 1]a$. (b) Band structure of the lattice with $t = t_1 = t_2 = 1$. (c) Band structure of the lattice with $t = 1$, $t_1 = 0.8$ and $t_2 = 1.2$. (d) Band structure of the lattice with $t = 1$, $t_1 = 1.2$ and $t_2 = 0.8$. The numbers in (b-d) illustrate the order of the bands.

Diagonalizing the Hamiltonian in Eq. (4), one obtains its eigenvalue b as a function of the Bloch momentum $\mathbf{k}$ and the corresponding eigenvectors $u_{\mathbf{k}}$. In Fig. 2(b), we show the band structure (viz. $b_{\mathbf{k}}$) of the lattice with $t = t_1 = t_2 = 1$, and one finds indeed two type-II Dirac cones between two neighboring bands. If $t_1 \neq t_2$, the corresponding band structures are displayed in

Optics EXPRESS

Figs. 2(c) and 2(d). One notes that band gaps have replaced Dirac points, and the band structures in Figs. 2(c) and 2(d) look the same. However, they are different in the Berry curvature.

The Berry curvature of a band is written as a pseudovector [75]:

$$\Omega_{n,\mathbf{k}} = \nabla_{\mathbf{k}} \times \mathcal{A}_{n,\mathbf{k}}, \tag{6}$$

where n is the band number, and:

$$\mathcal{A}_{n,\mathbf{k}} = i\langle u_{n,\mathbf{k}}| \frac{\partial}{\partial \mathbf{k}} |u_{n,\mathbf{k}}\rangle \tag{7}$$

is the Berry connection. The Berry curvatures of the three bands in Fig. 2(c) can be numerically obtained [76,77]; they are exhibited in Figs. 3(a)–3(c), and those corresponding to Fig. 2(d) are exhibited in Figs. 3(d)–3(f). Clearly, the Berry curvatures of the band structures in Figs. 2(c) and 2(d) are the opposite of each other. In addition, one may also calculate that the magnitudes of $|\Omega_{1\sim3,\mathbf{k}}|$ in the first Brillouin zone are π, 2π and π, which indicates that the valley Chern number of the valley with positive Berry curvature is $1/2$ and that of the valley with negative Berry curvature is $-1/2$. Therefore, VHE states are expected to occur at the domain wall that separates two inverted inversion-symmetry-broken lattices.

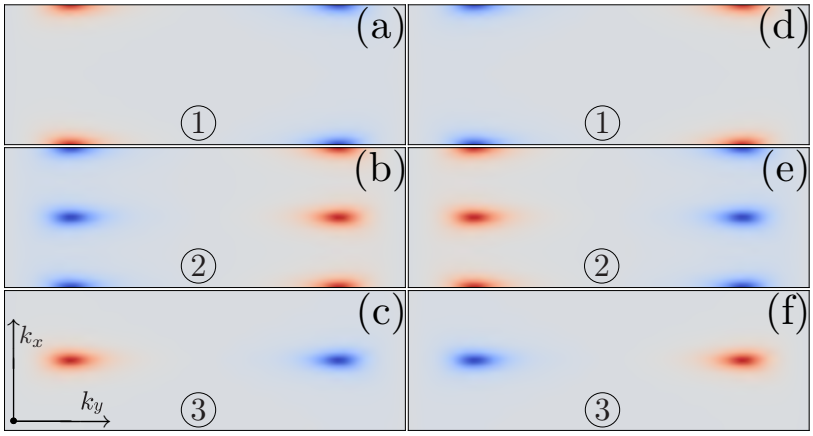

Fig. 3. Berry curvatures of the bands. (a-c) and (d-f) correspond respectively to the band structures in Fig. 2(c) and 2(d). The regions in blue represent a negative Berry curvature, while those in orange represent a positive one.

2.3. Valley Hall edge states

We now establish a domain wall based on the two different inversion-symmetry-broken lattices via distortion; one example is shown in Fig. 4(a), with the domain wall indicated by a red bracket. The corresponding band structure is shown in Fig. 4(b), and one finds VHE state in each band gap, quite close to the bulk band. VHE states at $k_y = 0$ are shown in Fig. 4(c). One finds that the energies of states are indeed mainly located on the domain wall, however they are not well localized, especially for the one in the upper band gap. What's more, VHE state is in-phase in the upper band gap and out-of-phase in the lower band gap, relative to an arbitrary initial phase; that is to say, they are always of the opposite phases relative to each other. As the distortion becomes stronger, the localization of the VHE state becomes better, see results in Figs. 4(d)–4(f) and Figs. 4(g)–4(i). In comparison with previous investigations [56,61], we find VHE states in both the top and the lower band gaps. In other words, for a given Bloch momentum, one expects two VHE states on the domain wall, which provides a lot of possibilities for preparing vector

Optics EXPRESS

VHE solitons. We believe that this is an indication of the advantage of the way to break the inversion symmetry of the lattice by distortion, rather then by detuning the refractive index change. Consequently, we choose the composite lattice are shown in Fig. 4(g) for further discussion.

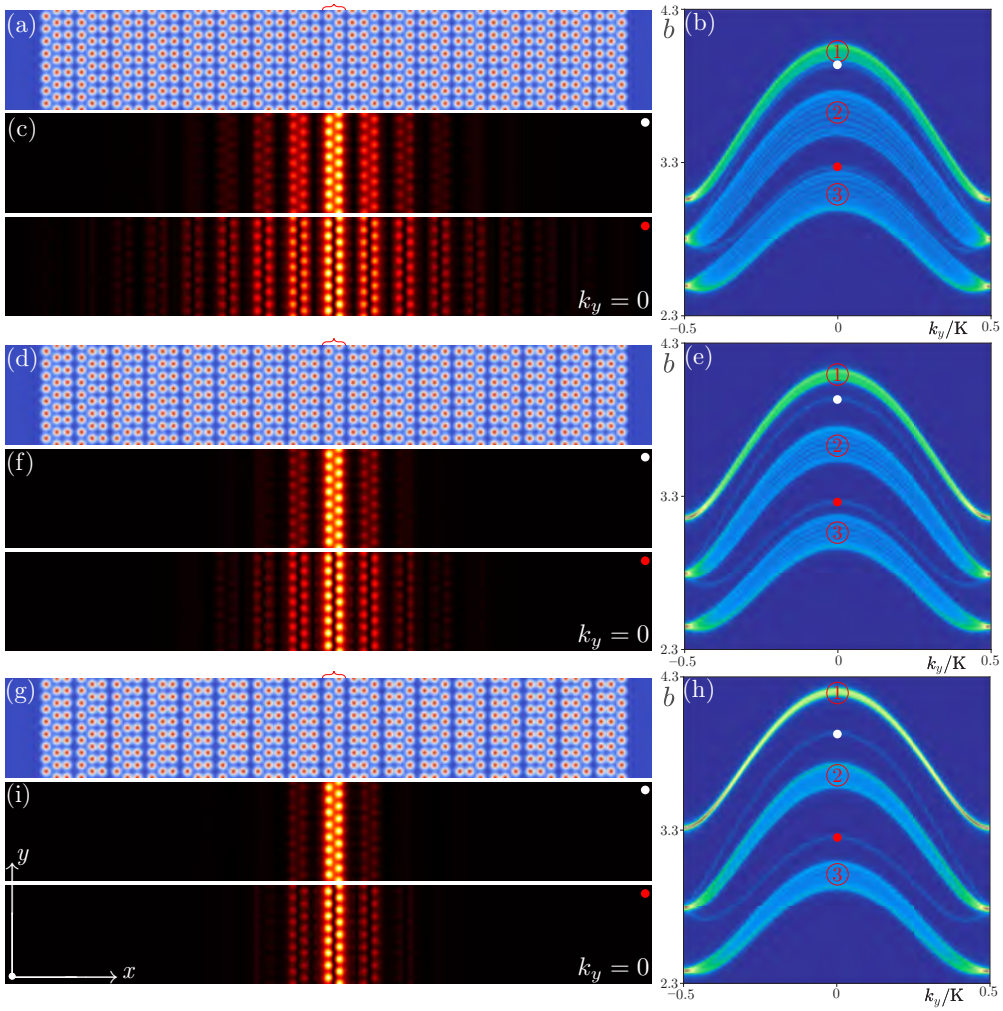

Fig. 4. (a) Composite type-II Dirac lattice with $a = 1.6$ and a domain wall highlighted by a red bracket on the top. Site B is closer to site A on the left-hand-side of the domain wall (separation is 1.5), and closer to site C on the right-hand-side of the domain wall. (b) The band structure $b(k_y)$ corresponding to structure (a). Two edge states can be seen within the two band gaps. They connect with the middle band at the Brillouin zone boundary and are in close proximity to the other two bands in the middle of the Brillouin zone. (c) VHE states at $k_y = 0$. The state shown in the top panel is from the VHE state in the upper band gap (white dot between bands 1 and 2), while that shown in the bottom panel is from the VHE state in the lower band gap (red dot between bands 2 and 3). (d-f) Arrangement is the same as in (a-c), but the separation between two closer sites is 1.4. (g-i) Arrangement is the same as in (a-c), but the separation between two closer sites is 1.3. Note that the edge states in (e, h) are well isolated from bulk bands, and therefore are well localized as shown in (f, i).

To seek more intricate properties of these edge states, the first-order derivative $b' = db/dk_y$ (group velocity) and the second-order derivative $b'' = d^2b/dk_y^2$ (dispersion) are calculated, and

Optics EXPRESS

the result is given in Fig. 5(a), where b' and b'' associated with the VHE states from the upper band gap are shown in red, while those associated with the lower band gap shown in blue. One finds that in the vicinity of the middle of the first Brillouin zone, b'' is negative for both upper and lower VHE states. This characteristic is essential in the formation of bright-bright vector solitons and bright-dipole vector solitons, which are discussed in the following subsection.

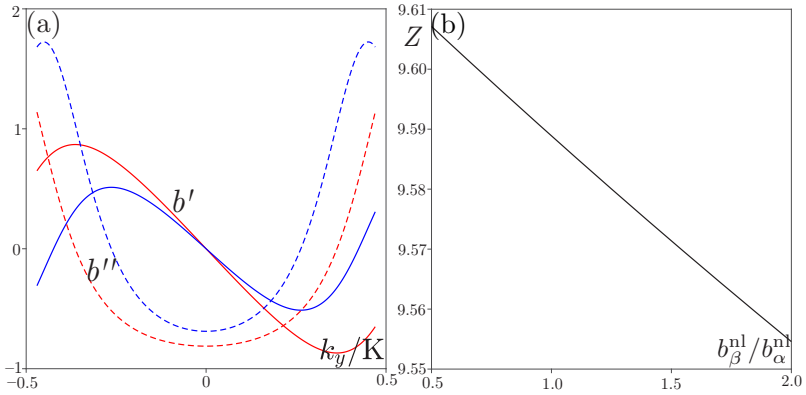

Fig. 5. (a) First-order derivative b' (solid curves) and second-order derivative b'' (dashed curves) of the valley Hall edge states in the top (red curves) and the bottom (blue curves) band gaps. (b) Dependence of the period Z of the bright-bright vector soliton on $b_\beta^{\rm nl}/b_\alpha^{\rm nl}$.

2.4. *Valley Hall edge solitons*

To construct vector VHE solitons, we follow the approach utilized in the previous literature [52,55], and consider bifurcation from the linear Bloch states. We are looking for the vector topological edge solitons, so we assume a solution in the form

$$\psi = A_\alpha(Y,z)\phi_\alpha \exp(ib_\alpha z) + A_\beta(Y,z)\phi_\beta \exp(ib_\beta z), \tag{8}$$

where $A_{\alpha,\beta}$ are the slowly-varying amplitudes and $Y = y - v_{\alpha,\beta}z$ is the coordinate in the frame of reference moving with velocity $v_{\alpha,\beta} = -b'_{\alpha,\beta}$ for both components. The evolution of the envelopes is then governed by the coupled nonlinear Schrödinger equations:

$$\begin{aligned} i\frac{\partial A_\alpha}{\partial z} &= \frac{b''_\alpha}{2}\frac{\partial^2 A_\alpha}{\partial Y^2} - \left(\chi_\alpha|A_\alpha|^2 + 2\chi|A_\beta|^2\right)A_\alpha, \\ i\frac{\partial A_\beta}{\partial z} &= \frac{b''_\beta}{2}\frac{\partial^2 A_\beta}{\partial Y^2} - \left(\chi_\beta|A_\beta|^2 + 2\chi|A_\alpha|^2\right)A_\beta, \end{aligned} \tag{9}$$

where $\chi_\nu = \langle|\phi_\nu|^2,|\phi_\nu|^2\rangle$ and $\chi = \langle|\phi_\alpha|^2,|\phi_\beta|^2\rangle$. The inner product $\langle f,g\rangle := \int_S f^* g dxdy$ is performed over the entire array area S. Numerically, Eq. (9) can be solved by using Newton's method in the form $A_\nu(Y,z) = w_\nu(Y)\exp(ib_\nu^{\rm nl}z)$ with $\nu = \alpha,\beta$, where $b_\nu^{\rm nl}$ is the nonlinearity-induced phase shift, which should be sufficiently small to make sure that the profile $w_\nu(Y)$ is broad and fulfills the slowly-varying envelope requirements.

First of all, we seek for the bright-bright vector VHE solitons. We choose the Bloch momentum $k_y = -0.12$K for VHE state in the upper band gap, and $k_y = -0.15$K for the one in the lower band gap, because they bear nearly the same velocities $v = -b' \sim -0.375$, according to the result in Fig. 5(a). Exemplary envelopes for the bright-bright vector solitons with $b_\alpha^{\rm nl} = 0.0020$ and $b_\beta^{\rm nl} = 0.0025$ are shown in Fig. 6(a). For a given $b_\alpha^{\rm nl}$, one can find numerous $b_\beta^{\rm nl}$ within the range $b_\beta^{\rm low} < b_\beta^{\rm nl} < b_\beta^{\rm upp}$ to form bright-bright vector solitons, as shown in Fig. 6(b). One finds that the

Optics EXPRESS

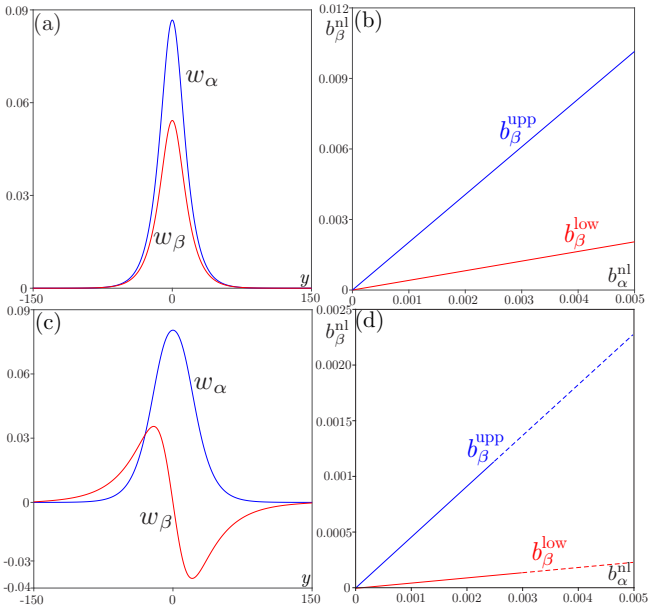

Fig. 6. (a) Envelopes of the components of bright-bright vector soliton with $b_\alpha^{\rm nl} = 0.0020$ and $b_\beta^{\rm nl} = 0.0025$. (b) Existence domain $b_\beta^{\rm low} < b_\beta^{\rm nl} < b_\beta^{\rm upp}$ of the bright-dipole vector soliton obtained for different $b_\alpha^{\rm nl}$. (c,d) Envelopes and the existence domain for bright-dipole vector soliton with $b_\alpha^{\rm nl} = 0.0015$ and $b_\beta^{\rm nl} = 0.0005$. Parameters for the component based on the VHE state in the lower band gap: $k_{y,\alpha} = -0.15$K and $b_\alpha'' = -0.5241$. Parameters for the component based on the VHE state in the upper band gap: $k_{y,\beta} = -0.12$K and $b_\beta'' = -0.7674$. Effective nonlinear coefficients for this choice of $k_{y,\alpha}$, $k_{y,\beta}$ are $\chi_\alpha = 0.3022$, $\chi_\beta = 0.3016$ and $\chi = 0.2837$. Solid curves in (b,d) mean the vector solitons are metastable, while dashed curves mean unstable vector solitons. The separation value in (d) is $b_\alpha^{\rm nl} = 0.0025$ for the upper boundary and $b_\alpha^{\rm nl} = 0.0030$ for the lower boundary.

upper and lower boundaries $b_\beta^{\rm upp,low}$ exhibit a linear behavior with $b_\alpha^{\rm nl}$. Even though bright-bright vector solitons have been reported previously [61], the bright-bright vector soliton reported here is different, since the two components that come from two different band gaps are in-phase and out-of-phase, respectively.

To our surprise, this composite lattice also supports bright-dipole vector solitons on its domain wall, and exemplary envelopes are shown in Fig. 6(c), with the existence domain displayed in Fig. 6(d). It should be noted that dipole vector solitons have been reported previously in both inversion-symmetry-broken lattices [60] and time-reversal-symmetry-broken lattices [55], however, here the edge is double-layered, instead of single layered in previous studies, and that brings completely novel phenomena that are not reported ever before.

We thus superpose the envelopes in Fig. 6(a) to the linear VHE states, to construct the bright-bright vector VHE solitons, and the propagation dynamics is shown in Fig. 7. The field modulus profiles of the vector soliton at certain propagation distances are selected and shown in Fig. 7(a). One finds that the beam moves along the negative y direction, which is in accordance with the prediction, and it does not broaden even when propagating up to $z \sim 5000$. If the nonlinearity in Eq. (1) is lifted, the beam broadens quickly during propagation, as shown by the field modulus profile at $z = 1600$ in Fig. 7(b). The comparison illustrates that the self-trapping of the beam is reached thanks to the effect of nonlinearity, and the bright-bright vector VHE soliton is thus demonstrated.

Optics EXPRESS

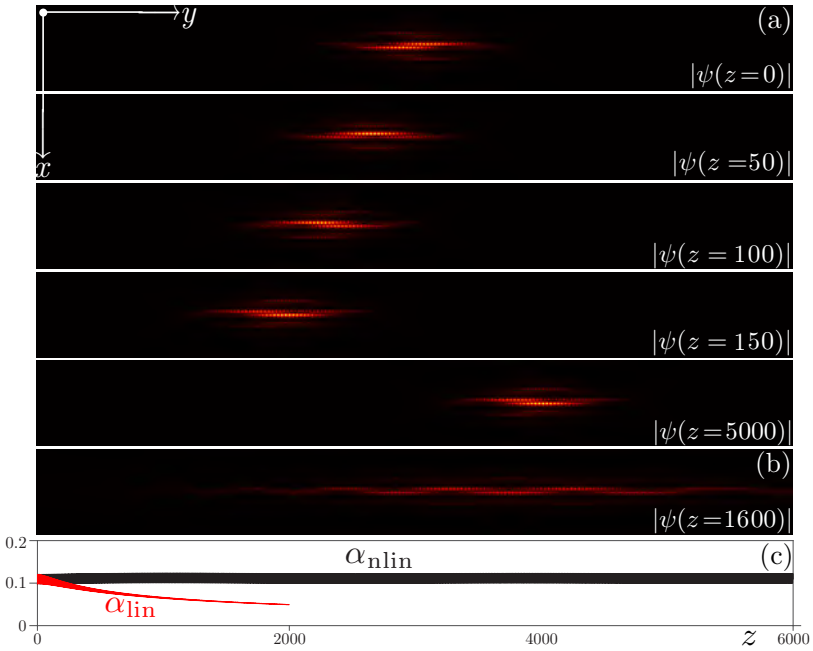

Fig. 7. Propagation dynamics of the bright-bright vector soliton (see Visualization 1). (a) Selected field modulus distributions of the soliton at different propagation distances. (b) Diffraction of the same input state as in (a) at $z = 1600$ in the absence of the nonlinear term in Eq. (1). (c) Peak amplitude of the beam during nonlinear (α_{nlin}) and linear (α_{lin}) propagation. Panels in (a) and (b) are shown in the window $-18 \le x \le 18$ and $-160 \le y \le 160$. Other parameters are the same as in Fig. 6(a).

We also record the peak amplitude of the beam during propagation, as shown in Fig. 7(c). During nonlinear propagation, the peak amplitude α_{nlin} exhibits a periodic property and does not decay. However, the peak amplitude α_{lin} in the linear propagation decays quickly. In addition, we also find that the beam structure displays periodic behavior during propagation—its profile changes periodically in Fig. 7(a), and this is why its peak amplitude α_{nlin} also behaves periodically. Initially, one half of the total energy of the beam is in the top layer and one half in the bottom layer, and the bottom layer is in front of the top layer. When the beam propagates to $z = 50$, almost all of the energy is transferred to the top layer. After further propagation to $z = 100$ that has experienced several periods, the energy is distributed equally in both layers again, but the top layer this time is in front of the bottom layer. The energy is almost all in the bottom layer, when the beam propagates to $z = 150$. One surmises that the energy distribution of the beam at $z = 200$ is similar to that at $z = 0$. The process repeats during propagation, exhibiting an oscillatory behavior. A detailed example of the propagation dynamics can be found in the associated Visualization 1, and the periodic behavior of the beam during propagation is more clearly visible there.

The reason for this peculiar periodic property of the vector soliton, with the components performing a competitive race during propagation, is that VHE state from the upper band gap is in-phase and that from the lower band gap is out-of-phase, causing the energy of the soliton to oscillate between the layers. Numerical simulations demonstrate that the period Z is affected by $b_\beta^{\mathrm{nl}}/b_\alpha^{\mathrm{nl}}$ slightly, as shown in Fig. 5(b). With the value of $b_\beta^{\mathrm{nl}}/b_\alpha^{\mathrm{nl}}$ increasing, the period Z decreases slightly. Anyway, the period is ~ 10; that explains why the beam at $z = 200$ is similar

Optics EXPRESS

to that at $z = 0$. Although the period changes a bit, the structure of the vector soliton does not change much, even after the propagation distance reaches $z \sim 5000$.

Following the same procedure, the bright-dipole vector VHE soliton can be obtained, and the propagation dynamics is shown in Fig. 8, as well as in the associated Visualization 2. During propagation, the profile of the bright-dipole vector VHE state also changes periodically.

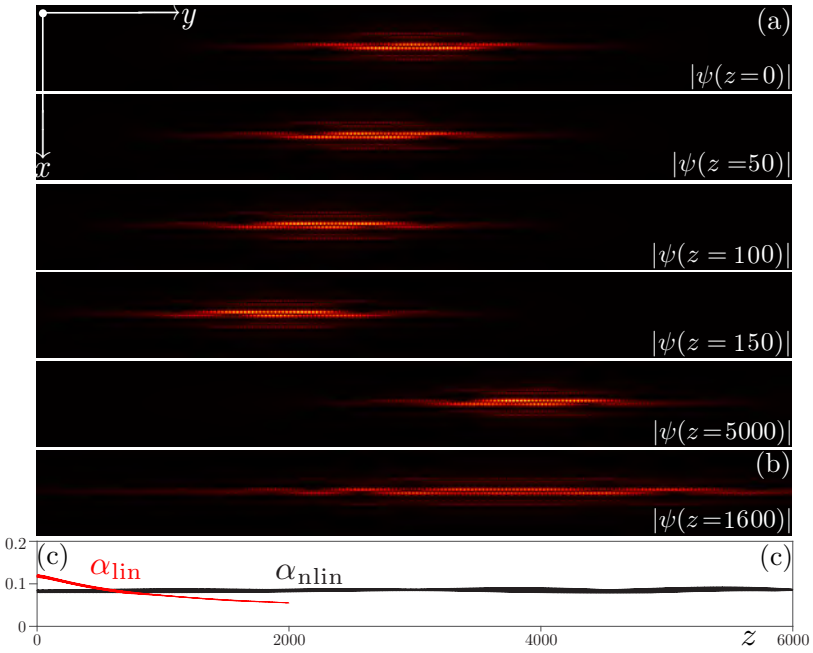

Fig. 8. Propagation dynamics of the bright-dipole vector soliton (see Visualization 2). (a) Selected field modulus distributions for the soliton at different propagation distances. (b) Diffraction of the same input state as in (a) at $z = 1600$ in the absence of nonlinearity in Eq. (1). (c) Peak amplitude of the beam during nonlinear ($\alpha_{\rm nlin}$) and linear ($\alpha_{\rm lin}$) propagation. Panels in (a) and (b) are shown in the window $-18 \le x \le 18$ and $-160 \le y \le 160$. Other parameters are the same as in Fig. 6(c).

3. Conclusion

Summarizing, we have reported the discovery of vector valley Hall edge solitons in distorted type-II Dirac photonic lattices. The distortion is achieved by moving one site relative to the others in the lattice's unit cell, resulting in the breaking of its inversion symmetry and the replacement of two type-II Dirac points by two band gaps. This creates a domain wall with two layers within the distorted lattice, which enables the existence of VHE states that are demonstrated by Berry curvatures. We have observed that the VHE state in the upper band gap is in-phase, while the one in the lower band gap is out-of-phase relative to an arbitrary initial phase. By superposing soliton envelopes onto the VHE states, we were able to generate both bright-bright and bright-dipole vector VHE solitons. During propagation, the energy of these vector solitons oscillates between the two layers of the domain wall, resulting in the periodic behavior of their profiles. Such a new type of vector topological solitons is not limited to photonic systems only; they can occur in any nonlinear topological systems where the interfaces/edges are double-layered.

Funding. National Natural Science Foundation of China (12074308, 91950120, U1537210); Qatar National Research Fund (13S-00121-200126).

Optics EXPRESS

Disclosures. The authors declare no conflicts of interest.

Data availability. Data underlying the results presented in this paper are not publicly available at this time but may be obtained from the authors upon reasonable request.

References

1. M. Z. Hasan and C. L. Kane, "Colloquium: Topological insulators," Rev. Mod. Phys. **82**(4), 3045–3067 (2010).
2. X.-L. Qi and S.-C. Zhang, "Topological insulators and superconductors," Rev. Mod. Phys. **83**(4), 1057–1110 (2011).
3. M. C. Rechtsman, J. M. Zeuner, Y. Plotnik, Y. Lumer, D. Podolsky, F. Dreisow, S. Nolte, M. Segev, and A. Szameit, "Photonic Floquet topological insulators," Nature **496**(7444), 196–200 (2013).
4. Z. Wang, Y. Chong, J. D. Joannopoulos, and M. Soljačić, "Observation of unidirectional backscattering-immune topological electromagnetic states," Nature **461**(7265), 772–775 (2009).
5. N. H. Lindner, G. Refael, and V. Galitski, "Floquet topological insulator in semiconductor quantum wells," Nat. Phys. **7**(6), 490–495 (2011).
6. M. Hafezi, E. A. Demler, M. D. Lukin, and J. M. Taylor, "Robust optical delay lines with topological protection," Nat. Phys. **7**(11), 907–912 (2011).
7. L.-H. Wu and X. Hu, "Scheme for achieving a topological photonic crystal by using dielectric material," Phys. Rev. Lett. **114**(22), 223901 (2015).
8. Y. Yang, Z. Gao, H. Xue, L. Zhang, M. He, Z. Yang, R. Singh, Y. Chong, B. Zhang, and H. Chen, "Realization of a three-dimensional photonic topological insulator," Nature **565**(7741), 622–626 (2019).
9. Z. Yang, F. Gao, X. Shi, X. Lin, Z. Gao, Y. Chong, and B. Zhang, "Topological acoustics," Phys. Rev. Lett. **114**(11), 114301 (2015).
10. C. He, X. Ni, H. Ge, X.-C. Sun, Y.-B. Chen, M.-H. Lu, X.-P. Liu, and Y.-F. Chen, "Acoustic topological insulator and robust one-way sound transport," Nat. Phys. **12**(12), 1124–1129 (2016).
11. J. Lu, C. Qiu, L. Ye, X. Fan, M. Ke, F. Zhang, and Z. Liu, "Observation of topological valley transport of sound in sonic crystals," Nat. Phys. **13**(4), 369–374 (2017).
12. G. Ma, M. Xiao, and C. T. Chan, "Topological phases in acoustic and mechanical systems," Nat. Rev. Phys. **1**(4), 281–294 (2019).
13. R. Süsstrunk and S. D. Huber, "Observation of phononic helical edge states in a mechanical topological insulator," Science **349**(6243), 47–50 (2015).
14. S. D. Huber, "Topological mechanics," Nat. Phys. **12**(7), 621–623 (2016).
15. G. Jotzu, M. Messer, R. Desbuquois, M. Lebrat, T. Uehlinger, D. Greif, and T. Esslinger, "Experimental realisation of the topological Haldane model," Nature **515**(7526), 237–240 (2014).
16. A. V. Nalitov, D. D. Solnyshkov, and G. Malpuech, "Polariton $\mathbb{Z}$ topological insulator," Phys. Rev. Lett. **114**(11), 116401 (2015).
17. P. St-Jean, V. Goblot, E. Galopin, A. Lemaître, T. Ozawa, L. Le Gratiet, I. Sagnes, J. Bloch, and A. Amo, "Lasing in topological edge states of a one-dimensional lattice," Nat. Photonics **11**(10), 651–656 (2017).
18. S. Klembt, T. H. Harder, O. A. Egorov, K. Winkler, R. Ge, M. A. Bandres, M. Emmerling, L. Worschech, T. C. H. Liew, M. Segev, C. Schneider, and S. Höfling, "Exciton-polariton topological insulator," Nature **562**(7728), 552–556 (2018).
19. V. V. Albert, L. I. Glazman, and L. Jiang, "Topological properties of linear circuit lattices," Phys. Rev. Lett. **114**(17), 173902 (2015).
20. Y. Hadad, J. C. Soric, A. B. Khanikaev, and A. Alù, "Self-induced topological protection in nonlinear circuit arrays," Nat. Electron. **1**(3), 178–182 (2018).
21. L. Lu, J. D. Joannopoulos, and M. Soljačić, "Topological photonics," Nat. Photonics **8**(11), 821–829 (2014).
22. T. Ozawa, H. M. Price, A. Amo, N. Goldman, M. Hafezi, L. Lu, M. C. Rechtsman, D. Schuster, J. Simon, O. Zilberberg, and I. Carusotto, "Topological photonics," Rev. Mod. Phys. **91**(1), 015006 (2019).
23. D. Smirnova, D. Leykam, Y. Chong, and Y. Kivshar, "Nonlinear topological photonics," Appl. Phys. Rev. **7**(2), 021306 (2020).
24. Y. V. Kartashov and D. V. Skryabin, "Bistable topological insulator with exciton-polaritons," Phys. Rev. Lett. **119**(25), 253904 (2017).
25. W. Zhang, X. Chen, Y. V. Kartashov, D. V. Skryabin, and F. Ye, "Finite-dimensional bistable topological insulators: From small to large," Laser Photonics Rev. **13**(11), 1900198 (2019).
26. Y. Q. Zhang, Y. V. Kartashov, and A. Ferrando, "Interface states in polariton topological insulators," Phys. Rev. A **99**(5), 053836 (2019).
27. M. Jürgensen, S. Mukherjee, and M. C. Rechtsman, "Quantized nonlinear Thouless pumping," Nature **596**(7870), 63–67 (2021).
28. Q. Fu, P. Wang, Y. V. Kartashov, V. V. Konotop, and F. Ye, "Nonlinear Thouless pumping: Solitons and transport breakdown," Phys. Rev. Lett. **128**(15), 154101 (2022).
29. Q. Fu, P. Wang, Y. V. Kartashov, V. V. Konotop, and F. Ye, "Two-dimensional nonlinear Thouless pumping of matter waves," Phys. Rev. Lett. **129**(18), 183901 (2022).
30. Y. Lumer, M. C. Rechtsman, Y. Plotnik, and M. Segev, "Instability of bosonic topological edge states in the presence of interactions," Phys. Rev. A **94**(2), 021801 (2016).

Optics EXPRESS

31. Y. V. Kartashov and D. V. Skryabin, "Modulational instability and solitary waves in polariton topological insulators," Optica **3**(11), 1228–1236 (2016).
32. G. Harari, M. A. Bandres, Y. Lumer, M. C. Rechtsman, Y. D. Chong, M. Khajavikhan, D. N. Christodoulides, and M. Segev, "Topological insulator laser: Theory," Science **359**(6381), eaar4003 (2018).
33. M. A. Bandres, S. Wittek, G. Harari, M. Parto, J. Ren, M. Segev, D. N. Christodoulides, and M. Khajavikhan, "Topological insulator laser: Experiments," Science **359**(6381), eaar4005 (2018).
34. A. Dikopoltsev, T. H. Harder, E. Lustig, O. A. Egorov, J. Beierlein, A. Wolf, Y. Lumer, M. Emmerling, C. Schneider, S. Höfling, M. Segev, and S. Klembt, "Topological insulator vertical-cavity laser array," Science **373**(6562), 1514–1517 (2021).
35. B. Bahari, A. Ndao, F. Vallini, A. El Amili, Y. Fainman, and B. Kanté, "Nonreciprocal lasing in topological cavities of arbitrary geometries," Science **358**(6363), 636–640 (2017).
36. Y. V. Kartashov and D. V. Skryabin, "Two-dimensional topological polariton laser," Phys. Rev. Lett. **122**(8), 083902 (2019).
37. Y. Zeng, U. Chattopadhyay, B. Zhu, B. Qiang, J. Li, Y. Jin, L. Li, A. G. Davies, E. H. Linfield, B. Zhang, Y. Chong, and Q. J. Wang, "Electrically pumped topological laser with valley edge modes," Nature **578**(7794), 246–250 (2020).
38. H. Zhong, Y. D. Li, D. H. Song, Y. V. Kartashov, Y. Q. Zhang, Y. P. Zhang, and Z. Chen, "Topological valley Hall edge state lasing," Laser Photonics Rev. **14**(7), 2000001 (2020).
39. H. Zhong, Y. V. Kartashov, A. Szameit, Y. Li, C. Liu, and Y. Zhang, "Theory of topological corner state laser in Kagome waveguide arrays," APL Photonics **6**(4), 040802 (2021).
40. L. J. Maczewsky, M. Heinrich, M. Kremer, S. K. Ivanov, M. Ehrhardt, F. Martinez, Y. V. Kartashov, V. V. Konotop, L. Torner, D. Bauer, and A. Szameit, "Nonlinearity-induced photonic topological insulator," Science **370**(6517), 701–704 (2020).
41. Y. V. Kartashov, G. E. Astrakharchik, B. A. Malomed, and L. Torner, "Frontiers in multidimensional self-trapping of nonlinear fields and matter," Nat. Rev. Phys. **1**(3), 185–197 (2019).
42. B. A. Malomed and D. Mihalache, "Nonlinear waves in optical and matter-wave media: A topical survey of recent theoretical and experimental results," Rom. J. Phys. **64**, 106 (2019).
43. D. Mihalache, "Localized structures in optical and matter-wave media: A selection of recent studies," Rom. Rep. Phys. **73**, 403 (2021).
44. Y. Lumer, Y. Plotnik, M. C. Rechtsman, and M. Segev, "Self-localized states in photonic topological insulators," Phys. Rev. Lett. **111**(24), 243905 (2013).
45. S. Mukherjee and M. C. Rechtsman, "Observation of Floquet solitons in a topological bandgap," Science **368**(6493), 856–859 (2020).
46. O. Bleu, G. Malpuech, and D. D. Solnyshkov, "Robust quantum valley Hall effect for vortices in an interacting bosonic quantum fluid," Nat. Commun. **9**(1), 3991 (2018).
47. D. Leykam and Y. D. Chong, "Edge solitons in nonlinear-photonic topological insulators," Phys. Rev. Lett. **117**(14), 143901 (2016).
48. M. J. Ablowitz and J. T. Cole, "Tight-binding methods for general longitudinally driven photonic lattices: Edge states and solitons," Phys. Rev. A **96**(4), 043868 (2017).
49. D. R. Gulevich, D. Yudin, D. V. Skryabin, I. V. Iorsh, and I. A. Shelykh, "Exploring nonlinear topological states of matter with exciton-polaritons: Edge solitons in kagome lattice," Sci. Rep. **7**(1), 1780 (2017).
50. C. Li, F. Ye, X. Chen, Y. V. Kartashov, A. Ferrando, L. Torner, and D. V. Skryabin, "Lieb polariton topological insulators," Phys. Rev. B **97**(8), 081103 (2018).
51. D. A. Smirnova, L. A. Smirnov, D. Leykam, and Y. S. Kivshar, "Topological edge states and gap solitons in the nonlinear Dirac model," Laser Photonics Rev. **13**(12), 1900223 (2019).
52. S. K. Ivanov, Y. V. Kartashov, A. Szameit, L. Torner, and V. V. Konotop, "Vector topological edge solitons in Floquet insulators," ACS Photonics **7**(3), 735–745 (2020).
53. S. K. Ivanov, Y. V. Kartashov, L. J. Maczewsky, A. Szameit, and V. V. Konotop, "Edge solitons in Lieb topological Floquet insulator," Opt. Lett. **45**(6), 1459–1462 (2020).
54. S. K. Ivanov, Y. V. Kartashov, L. J. Maczewsky, A. Szameit, and V. V. Konotop, "Bragg solitons in topological Floquet insulators," Opt. Lett. **45**(8), 2271–2274 (2020).
55. S. K. Ivanov, Y. V. Kartashov, M. Heinrich, A. Szameit, L. Torner, and V. V. Konotop, "Topological dipole Floquet solitons," Phys. Rev. A **103**(5), 053507 (2021).
56. H. Zhong, S. Xia, Y. Zhang, Y. Li, D. Song, C. Liu, and Z. Chen, "Nonlinear topological valley Hall edge states arising from type-II Dirac cones," Adv. Photonics **3**(05), 056001 (2021).
57. D. A. Smirnova, L. A. Smirnov, E. O. Smolina, D. G. Angelakis, and D. Leykam, "Gradient catastrophe of nonlinear photonic valley-Hall edge pulses," Phys. Rev. Res. **3**(4), 043027 (2021).
58. B. Ren, H. Wang, V. O. Kompanets, Y. V. Kartashov, Y. Li, and Y. Zhang, "Dark topological valley Hall edge solitons," Nanophotonics **10**(13), 3559–3566 (2021).
59. Q. Tang, B. Ren, V. O. Kompanets, Y. V. Kartashov, Y. Li, and Y. Zhang, "Valley Hall edge solitons in a photonic graphene," Opt. Express **29**(24), 39755–39765 (2021).
60. Q. Tang, Y. Zhang, Y. V. Kartashov, Y. Li, and V. V. Konotop, "Vector valley Hall edge solitons in superhoneycomb lattices," Chaos, Solitons Fractals **161**, 112364 (2022).

Optics EXPRESS

61. Y. Tian, Y. Zhang, Y. Li, and M. R. Belić, "Vector valley Hall edge solitons in the photonic lattice with type-II Dirac cones," Front. Phys. **17**(5), 53503 (2022).
62. H. Zhong, Y. V. Kartashov, Y. Li, and Y. Zhang, "π-mode solitons in photonic Floquet lattices," Phys. Rev. A **107**(2), L021502 (2023).
63. W. Zhang, X. Chen, Y. V. Kartashov, V. V. Konotop, and F. Ye, "Coupling of edge states and topological Bragg solitons," Phys. Rev. Lett. **123**(25), 254103 (2019).
64. F. Zangeneh-Nejad and R. Fleury, "Nonlinear second-order topological insulators," Phys. Rev. Lett. **123**(5), 053902 (2019).
65. M. S. Kirsch, Y. Zhang, M. Kremer, L. J. Maczewsky, S. K. Ivanov, Y. V. Kartashov, L. Torner, D. Bauer, A. Szameit, and M. Heinrich, "Nonlinear second-order photonic topological insulators," Nat. Phys. **17**(9), 995–1000 (2021).
66. Z. Hu, D. Bongiovanni, D. Jukić, E. Jajtić, S. Xia, D. Song, J. Xu, R. Morandotti, H. Buljan, and Z. Chen, "Nonlinear control of photonic higher-order topological bound states in the continuum," Light: Sci. Appl. **10**(1), 164 (2021).
67. Y. V. Kartashov, A. A. Arkhipova, S. A. Zhuravitskii, N. N. Skryabin, I. V. Dyakonov, A. A. Kalinkin, S. P. Kulik, V. O. Kompanets, S. V. Chekalin, L. Torner, and V. N. Zadkov, "Observation of edge solitons in topological trimer arrays," Phys. Rev. Lett. **128**(9), 093901 (2022).
68. D. Tan, Z. Wang, B. Xu, and J. Qiu, "Photonic circuits written by femtosecond laser in glass: improved fabrication and recent progress in photonic devices," Adv. Photonics **3**(02), 024002 (2021).
69. L. Li, W. Kong, and F. Chen, "Femtosecond laser-inscribed optical waveguides in dielectric crystals: a concise review and recent advances," Adv. Photonics **4**(02), 024002 (2022).
70. Z. Lin and M. Hong, "Femtosecond laser precision engineering: From micron, submicron, to nanoscale," Ultrafast Sci. **2021**, 9783514 (2021).
71. K. C. Jin, H. Zhong, Y. D. Li, F. W. Ye, Y. P. Zhang, F. L. Li, C. L. Liu, and Y. Q. Zhang, "Parametric type-II Dirac photonic lattices," Adv. Quantum Technol. **3**(7), 2000015 (2020).
72. Q. Tang, B. Ren, M. R. Belić, Y. Zhang, and Y. Li, "Valley Hall edge solitons in the kagome photonic lattice," Rom. Rep. Phys. **74**(24), 405 (2022).
73. J. Noh, S. Huang, K. P. Chen, and M. C. Rechtsman, "Observation of photonic topological valley Hall edge states," Phys. Rev. Lett. **120**(6), 063902 (2018).
74. X. Wu, Y. Meng, J. Tian, Y. Huang, H. Xiang, D. Han, and W. Wen, "Direct observation of valley-polarized topological edge states in designer surface plasmon crystals," Nat. Commun. **8**(1), 1304 (2017).
75. D. Xiao, M.-C. Chang, and Q. Niu, "Berry phase effects on electronic properties," Rev. Mod. Phys. **82**(3), 1959–2007 (2010).
76. T. Fukui, Y. Hatsugai, and H. Suzuki, "Chern numbers in discretized Brillouin zone: Efficient method of computing (spin) Hall conductances," J. Phys. Soc. Jpn. **74**(6), 1674–1677 (2005).
77. J. N. Fuchs, F. Piéchon, M. O. Goerbig, and G. Montambaux, "Topological Berry phase and semiclassical quantization of cyclotron orbits for two dimensional electrons in coupled band models," Eur. Phys. J. B **77**(3), 351–362 (2010).